A feedback-feed-forward steering control strategy for improving lateral dynamics stability of an A-double vehicle at high speeds

Citation for the original published paper (version of record):
Sadeghi Kati, M., Fredriksson, J., Jacobson, B. et al (2021)
A feedback-feed-forward steering control strategy for improving lateral dynamics stability of an A-double vehicle at high speeds
Vehicle System Dynamics, In Press
http://dx.doi.org/10.1080/00423114.2021.1988117

VEHICLE SYSTEM DYNAMICS
https://doi.org/10.1080/00423114.2021.1988117

A feedback-feed-forward steering control strategy for improving lateral dynamics stability of an A-double vehicle at high speeds

Maliheh Sadeghi Kati [a], Jonas Fredriksson [a], Bengt Jacobson [b] and Leo Laine [c]

[a]Electrical Engineering Department, Chalmers University of Technology, Gothenburg, Sweden; [b]Department of Mechanics and Maritime Sciences, Chalmers University of Technology, Gothenburg, Sweden; [c]Vehicle Automation, Volvo Group Trucks Technology, Gothenburg, Sweden

ABSTRACT

A control strategy based on $\mathcal{H}_\infty$-type static output feedback combined with dynamic feed-forward is proposed to improve the high-speed lateral performance of an A-double combination vehicle (tractor–semitrailer–dolly–semitrailer) using active steering of the front axle of the dolly. Both feedback and feed-forward syntheses are performed via Linear Matrix Inequality (LMI) optimisation. From a practical point of view, the proposed controller is simple and easy to implement, despite its theoretical complexity. In fact, the measurement of the driver steering angle and only one articulation angle are required for the feed-forward and the feedback controllers, respectively. The results are verified using a high-fidelity vehicle model and confirm a significant reduction in yaw rate and lateral acceleration rearward amplification and also high-speed transient off-tracking, and subsequently improving the lateral stability and performance of the A-double combination vehicle during sudden lane change manoeuvres.

ARTICLE HISTORY
Received 1 April 2021
Revised 7 July 2021
Accepted 18 September 2021

KEYWORDS
Static output feedback; dynamic feed-forward; LMI-based $\mathcal{H}_\infty$ synthesis; rearward amplification; active dolly steering

1. Introduction

The use of active steering systems has shown a remarkable potential in improving manoeuvrability and lateral performance of long combination vehicles (LCVs). The active steering of towed units in heavy vehicles has been widely investigated to improve the low-speed manoeuvrability (e.g. [1–5]), high-speed lateral stability (e.g. [6–10]), and both the manoeuvrability and lateral stability (e.g. [11–18]). This paper focuses on dynamic stability improvement of a double-trailer-type LCV called "A-double combination vehicle", as shown in Figure 1. The A-double combination vehicle, briefly denoted as the A-double, consists of a tractor towing two semitrailers, linked together by a dolly. Instead of a trailer steering system as suggested in the literature (e.g. [19–21]), designing an active dolly steering system is more reasonable and practical from the economical point of view to improve the high-speed lateral dynamic stability and performance of the A-double due to the small

CONTACT Maliheh Sadeghi Kati maliheh.sadeghi.kati@chalmers.se

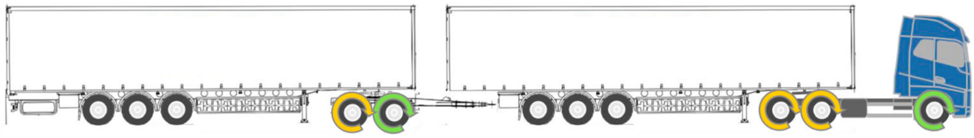

Figure 1. A-double vehicle schematic (steerable axles in green colour and propelled axles in yellow colour).

size of the dolly unit. In the previous works (see [22]) on active dolly steering, both axles of the dolly were considered steerable, while in this work only the front axle of the dolly is steerable, as can be seen in Figure 1. This type of electrically propelled dolly is called an intelligent dolly (i-dolly) and is aimed to automatically be connected to the next semi-trailer from the dry port and by recorded route paths drive to the designated logistic terminals.

In this paper, a synthesis based on static output feedback (SOFB) is considered instead of full-state feedback motivated by the fact that the measurement of some states might not be available for feedback or might require complicated installation processes, costly sensors and advanced estimation procedures. In this fashion, only one articulation angle that is relatively easy to measure is available which is the articulation angle between the first semitrailer and the dolly. The implementation of SOFB is quite easy in practice. In our case, for instance, the controller will be composed of a single gain block. Among the SOFB controller design methods (see e.g. [23] and the references therein), the approach proposed in [24] is adopted in which sufficient solvability conditions are expressed in the form of (dilated) linear matrix inequalities (LMI).

As the measurement of the driver steering angle input is available in addition to the articulation angle, a combined synthesis of SOFB controller with a feed-forward (FF) controller can further improve the vehicle dynamic performances. Hence, in this paper, a two-step design method is adopted. In the first step, an SOFB controller is designed in a way to maintain stability and optimise the performance objective as much as possible. In the second step, a dynamic feed-forward (DFF) controller is synthesised for the closed-loop system in a way to further optimise the performance objective. In this paper, a direct synthesis is suggested for DFF filters for a particular system structure in which there is a weighting filter in the disturbance input. In the used method, the approach proposed in [25] is used by a modification which is including the weighting filter for the external disturbance input. In this approach, the order and the pole(s) of the DFF filter are decided by the designer.

The paper is organised in a way to evolve from abstract problem formulation and the proposed design methods to the engineering problem that forms the underlying motivation. In the next section, an $\mathcal{H}_\infty$-type synthesis problem is formulated and then the solution is provided based on LMI optimisation. The application to the lateral control of the A-double is then explained in Section 3 by discussing the vehicle and driver model as well as the formulation of the performance objectives. Then a number of example designs are presented together with the associated simulation results in order to illustrate the potential improvements offered by the proposed approaches. The paper is then concluded with some final remarks in Section 4.

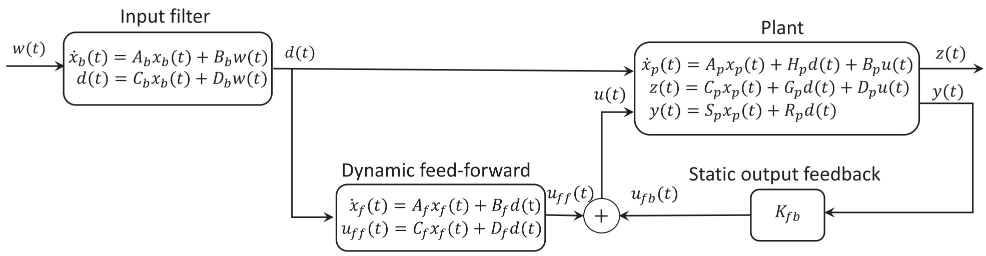

Figure 2. Block diagram of combined SOFB and DFF.

2. Combined static output feedback and dynamic feed-forward control design

In this section, a combined SOFB and DFF control synthesis procedure is proposed based on LMI optimisation in order to ensure stability as well as a desired output performance. The configuration of the control system considered in this paper is displayed in Figure 2.

The linear time-invariant (LTI) vehicle model is represented with a state-space realisation as

$$\begin{cases} \dot{x}_p(t) = A_p\, x_p(t) + H_p\, \mathrm{d}(t) + B_p\, u(t), \\ z(t) = C_p\, x_p(t) + G_p\, \mathrm{d}(t) + D_p\, u(t), \\ y(t) = S_p\, x_p(t) + R_p\, \mathrm{d}(t), \end{cases} \tag{1}$$

where $x_p(t) \in \mathbb{R}^{n_p}$ represents the state vector, $u(t) \in \mathbb{R}^{n_u}$ denotes the control input, $d(t) \in \mathbb{R}^{n_d}$ is a measurable disturbance, $y(t) \in \mathbb{R}^{n_y}$ is the measured output containing the available states of the system for feedback and $z(t) \in \mathbb{R}^{n_z}$ is a signal based on which performance is to be evaluated. The matrices C_p, G_p and D_p will be determined depending on the considered performance output $z(t)$. The matrices S_p and R_p will be defined based on the available measurements.

The measurable disturbance in the system is the driver steering input. In order to model the driver behaviour, the measurable disturbance $d(t)$ is assumed to be generated by an input weighting filter of the form

$$\begin{cases} \dot{x}_b(t) = A_b\, x_b(t) + B_b\, w(t), \\ d(t) = C_b\, x_b(t) + D_b\, w(t), \end{cases} \tag{2}$$

where $x_b(t) \in \mathbb{R}^{n_b}$ is the input filter state vector and $w(t) \in \mathbb{R}^{n_w}$ represents an artificial signal of finite-energy. With this filter, it is assumed that the frequency content of the driver steering is concentrated in a particular range of frequency. In fact, the use of a weighting filter is motivated by the fact that drivers will not provide arbitrary steering inputs. Indeed the manoeuvres will typically be initiated by smooth steering inputs as in real life, whose frequency contents would be limited to a certain frequency band.

In order to formulate the synthesis of a controller based on SOFB combined with DFF, the control input is hence formed as

$$u(t) = u_{fb}(t) + u_{ff}(t), \tag{3}$$

where $u_{fb}(t)$ and $u_{ff}(t)$ are the SOFB control and the DFF control signals, respectively. The feedback control signal $u_{fb}(t)$ is computed as

$$u_{fb}(t) = K_{fb}\, y(t), \tag{4}$$

where K_{fb} is the gain matrix to be designed. On the other hand, the DFF control signal $u_{ff}(t)$ is obtained by passing the measurable disturbance signal $d(t)$ through a dynamic filter described by

$$\begin{cases} \dot{x}_f(t) = A_f\, x_f(t) + B_f\, \mathrm{d}(t), \\ u_{ff}(t) = C_f\, x_f(t) + D_f\, \mathrm{d}(t), \end{cases} \tag{5}$$

where $x_f(t) \in \mathbb{R}^{n_f}$ is the filter state and (A_f, B_f, C_f, D_f) represents a realisation of the filter to be found.

The design procedure of SOFB and DFF decomposes the controller design process into two separate steps. In the first step, the SOFB gain K_{fb} is computed. This is then used to find a new state-space realisation for the closed-loop system in the absence of the DFF controller. This new state-space realisation is then used in the second step to compute the realisation matrices (A_f, B_f, C_f, D_f) of the DFF filter.

2.1. Static output feedback (SOFB) design

In this section, a procedure for $\mathcal{H}_\infty$ static output feedback synthesis is described. The objective of the $\mathcal{H}_\infty$ synthesis is to ensure bounds on the energy gain from the disturbance $d(t)$ to the performance output of the system $z(t)$. To this end, first the band-pass filter in (2) is added to the dynamics of the vehicle in (1). In this fashion, an extended version of the state-space realisation of the plant is obtained as follows:

$$\begin{cases} \dot{x}(t) = \underbrace{\begin{bmatrix} A_p & H_pC_b \\ 0 & A_b \end{bmatrix}}_{A} \underbrace{\begin{bmatrix} x_p(t) \\ x_b(t) \end{bmatrix}}_{x(t)} + \underbrace{\begin{bmatrix} H_pD_b \\ B_b \end{bmatrix}}_{H} w(t) + \underbrace{\begin{bmatrix} B_p \\ 0 \end{bmatrix}}_{B} u_{fb}(t), \\ z(t) = \underbrace{\begin{bmatrix} C_p & G_pC_b \end{bmatrix}}_{C} x(t) + \underbrace{G_pD_b}_{G}\, w(t) + \underbrace{D_p}_{D}\, u_{fb}(t), \\ y(t) = \underbrace{\begin{bmatrix} S_p & R_pC_b \end{bmatrix}}_{S} x(t) + \underbrace{R_pD_b}_{R}\, w(t), \end{cases} \tag{6}$$

where $x(t) \in \mathbb{R}^{n_x}$ with $n_x = n_p + n_b$.

In order to design the static feedback gain K_{fb} in (4), an LMI-based $\mathcal{H}_\infty$ output feedback design technique is now recalled from [24]. The $\mathcal{H}_\infty$ SOFB synthesis problem is hence formulated as follows: Given an LTI plant as in (6), find a feedback gain matrix $K_{fb} \in \mathbb{R}^{n_u \times n_y}$ such that the resulting closed-loop system is stable (i.e. $A + B\,K_{fb}\,S$ is Hurwitz) and satisfies the following condition for all disturbance signals $w(\cdot)$ with $0 < \|w\|_2 < \infty$ under zero initial condition:

$$\|z\|_2 \triangleq \sqrt{\int_0^\infty z(t)^T z(t)\,\mathrm{d}t} < \gamma\,\|w\|_2, \quad x(0) = 0. \tag{7}$$

In this expression, γ represents the level of guaranteed $\mathcal{L}_2$-gain performance and is desired to be minimised. In order to ensure the performance objective in (7), the approach proposed in [24] is used, which provides dilated LMI conditions for SOFB synthesis. The idea behind the dilation is to assume a feedback gain expressed in terms of two matrix variables N and W as

$$K_{fb} = N\,W^{-1}, \tag{8}$$

where W is assumed to be non-singular. In this fashion, the control input is decoupled from the Lyapunov matrix (denoted by Y) in order to reduce the potential conservatism. Referring the reader for further details to [24], the relevant solution is as follows: there is a solution if there exist matrix variables $0 \prec Y = Y^T \in \mathbb{R}^{n_x \times n_x}$, $W \in \mathbb{R}^{n_y \times n_y}$ and $N \in \mathbb{R}^{n_u \times n_y}$ for which

$$\mathrm{He}\begin{bmatrix} -\phi W & \phi(SY - WS) & \phi R & 0 \\ BN & AY + BNS & H & 0 \\ 0 & 0 & -\frac{\gamma}{2} I & 0 \\ DN & CY + DNS & G & -\frac{\gamma}{2} I \end{bmatrix} \prec 0, \tag{9}$$

where $\mathrm{He}\,\mathcal{N} \triangleq \mathcal{N} + \mathcal{N}^T$ and $\phi \in \mathbb{R}_+$ is an arbitrary (yet fixed) scalar. The SOFB gain matrix is then computed as in (8). Note that (9) is an LMI condition only with fixed ϕ. In order to find the minimum possible value of γ under this condition, one needs to perform a line search over ϕ. More clearly, one needs to minimise γ for each fixed ϕ over a certain grid of ϕ values and then picks the design in which the smallest γ is obtained; see [26].

For DFF synthesis, a realisation of the plant is now derived with fixed SOFB. It is hence assumed that $u_{fb}(t)$ is computed with a known K_{fb} as in (4) and then (3) is inserted in the realisation of the plant given by (1). This leads to a new state-space realisation of the closed-loop system (i.e. the plant under SOFB) as

$$\begin{cases} \dot{x}_p(t) = \underbrace{(A_p + B_p K_{fb} S_p)}_{A_c} x_p(t) + \underbrace{(H_p + B_p K_{fb} R_p)}_{H_c} \mathrm{d}(t) + B_p u_{ff}(t), \\ z(t) = \underbrace{(C_p + D_p K_{fb} S_p)}_{C_c} x_p(t) + \underbrace{(G_p + D_p K_{fb} R_p)}_{G_c} \mathrm{d}(t) + D_p u_{ff}(t), \end{cases} \tag{10}$$

where $u_{ff}(t)$ represents the DFF control input to be designed in the sequel for further performance improvement.

2.2. Dynamic feed-forward (DFF) design

In this section, the problem of DFF synthesis is considered for the closed-loop system identified by (10) in the previous subsection. Here the synthesis goal is to compute a realisation

(A_f, B_f, C_f, D_f) of the DFF filter presented in (5). The transfer function of the DFF filter is given by

$$\mathcal{K}_{ff}(s) \triangleq C_f(sI - A_f)^{-1}B_f + D_f. \tag{11}$$

The DFF design problem is now formulated as follows: given the closed-loop system in (10), find a DFF filter as in (11) such that the performance condition in (7) is ensured. Note that the DFF synthesis problem is also formulated with the same performance objective where γ represents the guaranteed level of performance. After the SOFB synthesis is performed by minimising γ, the DFF synthesis will also be performed with such a minimisation with fixed SOFB gain. It is desired to achieve a smaller γ (i.e. improved performance) in the optimisation for DFF synthesis. In order to obtain a tractable formulation of the DFF synthesis, a derivation of LMI conditions is needed that ensure (7) for the system of (10).

In the DFF synthesis method, the approach proposed in [25] is modified in a way to take into account the weighting filter for external disturbances given in (2). The matrices (A_f, B_f) are considered to be fixed while C_f and D_f are to be designed and the following realisation is used for the DFF filter expressed as

$$\begin{bmatrix} A_f & B_f \\ C_f & D_f \end{bmatrix} = \left[\begin{array}{cccccc|c} -\psi I & I & 0 & \cdots & 0 & 0 \\ 0 & -\psi I & I & \cdots & 0 & 0 \\ \vdots & \vdots & \ddots & \ddots & \vdots & \vdots \\ 0 & 0 & \ddots & -\psi I & I & 0 \\ 0 & 0 & \cdots & \cdots & -\psi I & I \\ C_f^l & C_f^{l-1} & \cdots & C_f^2 & C_f^1 & D_f \end{array}\right]. \tag{12}$$

where the scalar $-\psi$ represents the pole of the DFF filter, which is repeated l times. The transfer function of this DFF filter is given by

$$\mathcal{K}_{ff}(s) = D_f + \sum_{i=1}^{l} {C_f}^i (s + \psi)^{-i}. \tag{13}$$

It should be noted that the positive scalar $\psi > 0$ and the integer $l \geq 1$ need to be chosen beforehand by the designer so that (A_f, B_f) can then be treated as fixed. It should be noted that a single repeated pole is chosen for the DFF filter since it was quiet convenient from a design point of view, although it is also possible to choose different poles as well.

In order to reformulate the problem as in [25], the dynamics of the weighting filter in (2) is first combined with the dynamics of the DFF filter in (5) as

$$\begin{cases} \dot{\hat{x}}_f(t) = \underbrace{\begin{bmatrix} A_b & 0 \\ B_f C_b & A_f \end{bmatrix}}_{\hat{A}_f} \underbrace{\begin{bmatrix} x_b(t) \\ x_f(t) \end{bmatrix}}_{\hat{x}_f(t)} + \underbrace{\begin{bmatrix} B_b \\ B_f D_b \end{bmatrix}}_{\hat{B}_f} w(t), \\ u_{ff}(t) = \underbrace{\begin{bmatrix} D_f C_b & C_f \end{bmatrix}}_{\hat{C}_f} \hat{x}_f(t) + \underbrace{D_f D_b}_{\hat{D}_f} w(t), \end{cases} \tag{14}$$

where $\hat{x}_f(t) \in \mathbb{R}^{n_{\hat{f}}}$ with $n_{\hat{f}} = n_f + n_b$. Next the dynamics of the closed-loop plant from (10) is re-expressed by replacing $d(t)$ with the expression given in (2) as

$$\begin{cases} \dot{x}_p(t) = A_c x_p(t) + \underbrace{\begin{bmatrix} H_c C_b & 0 \end{bmatrix}}_{\hat{H}_b} \hat{x}_f(t) + H_c D_b w(t) + B_p u_{ff}(t), \\ z(t) = C_c x_p(t) + \underbrace{\begin{bmatrix} G_c C_b & 0 \end{bmatrix}}_{\hat{G}_b} \hat{x}_f(t) + G_c D_b w(t) + D_p u_{ff}(t), \end{cases} \tag{15}$$

and, thereby, the extended matrices $\hat{H}_b$ and $\hat{G}_b$ are introduced. In order to derive LMI conditions for DFF synthesis, let us first recall from [27] the matrix inequality conditions that ensure (7) as follows:

$$\mathscr{Y}^T \mathscr{X} \mathscr{Y} \succ 0, \tag{16}$$

$$\text{He} \begin{bmatrix} \mathscr{Y}^T(\mathscr{X}\mathscr{A})\mathscr{Y} & \mathscr{Y}^T(\mathscr{X}\mathscr{B}) & 0 \\ 0 & -\frac{\gamma}{2} I & 0 \\ \mathscr{C}\mathscr{Y} & \mathscr{D} & -\frac{\gamma}{2} I \end{bmatrix} \prec 0. \tag{17}$$

Based on the approach in [25], $\mathscr{X}$ and $\mathscr{Y}$ are chosen in the $\mathcal{H}_\infty$ performance conditions of (16) and (17) as

$$\mathscr{X} = \underbrace{\begin{pmatrix} Y & V \\ 0 & I \end{pmatrix}^{-T}}_{\mathcal{Y}^{-T}} \begin{pmatrix} I & -V \\ 0 & X \end{pmatrix}. \tag{18}$$

By performing derivations in a similar way to [25], the following result is obtained: There is a solution to DFF problem, if there exist $0 \prec Y = Y^T \in \mathbb{R}^{n_p \times n_p}$, $0 \prec X = X^T \in \mathbb{R}^{n_{\hat{f}} \times n_{\hat{f}}}$, $V \in \mathbb{R}^{n_p \times n_{\hat{f}}}$, $C_f \in \mathbb{R}^{n_u \times n_f}$ and $D_f \in \mathbb{R}^{n_u \times n_d}$ that satisfy

$$\text{He} \begin{bmatrix} A_c Y & \hat{H}_b + A_c V + B_p \hat{C}_f - V\hat{A}_f & H_c D_b + B_p \hat{D}_f - V\hat{B}_f & 0 \\ 0 & X\hat{A}_f & X\hat{B}_f & 0 \\ 0 & 0 & -\frac{\gamma}{2} I & 0 \\ C_c Y & \hat{G}_b + C_c V + D_p \hat{C}_f & G_c D_b + D_p \hat{D}_f & -\frac{\gamma}{2} I \end{bmatrix} \prec 0. \tag{19}$$

The DFF filter can then be constructed with (A_f, B_f) chosen as in (12) and with (C_f, D_f) obtained directly from the LMI optimisation.

3. Application to the lateral control of the A-double combination vehicle

In this section, the synthesis method developed in the previous section will be applied to control lateral dynamic of the A-double at high speeds. The A-double vehicle has a total weight of 76 tons and a total length of about 32 m. The control is performed by favour of

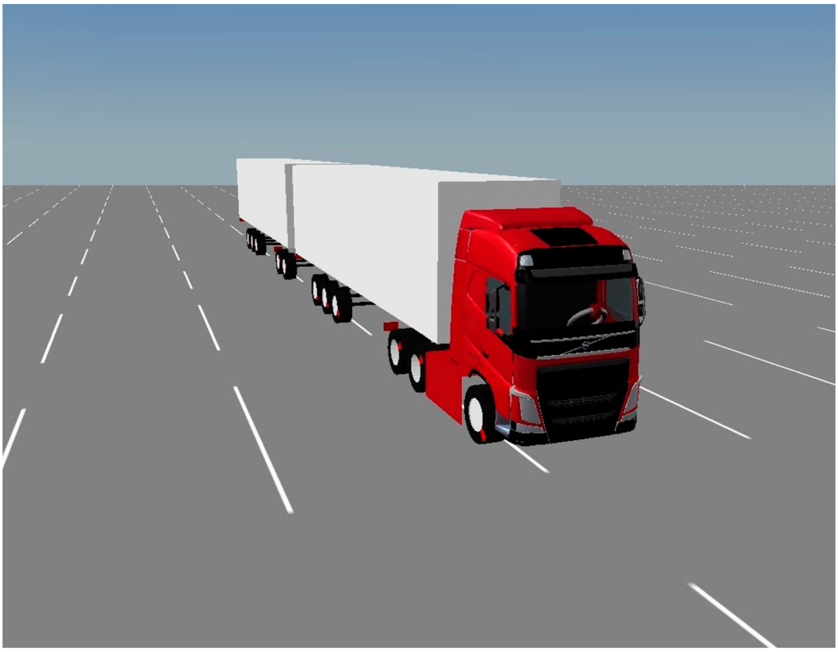

Figure 3. VTM model of the A-double.

first axle of the dolly, while the other axles of the vehicle remain unchanged. In order to evaluate the designed controller, a high-fidelity nonlinear model is used, which is briefly explained first. This is followed by a detailed description of the linear model used for the vehicle including the dolly steering actuator as well as the driver. As required in the generalised plant description, the signal used for performance evaluation is also specified.

3.1. Nonlinear vehicle model

The high-fidelity, nonlinear vehicle model of the A-double considered in this paper is developed by Volvo Group Trucks Technology, henceforth referred to as the VTM (Volvo Transport Models) model [28,29], see Figure 3. The VTM model contains detailed sub-models of the complete combination vehicle including frames, tyres, axles, steering system, suspensions, and brakes which are modelled in Simscape Multibody™ in Simulink®. In this vehicle model, the tyre characteristics are modelled by using the Magic Formula of Pacejka [30], called `PAC2002`. The VTM model of the A-double includes four units where all the units are constructed using two rigid bodies with a torsional viscoelasticity type connection. The VTM library has been tested and validated against real test data and proved to be sufficiently accurate in predicting the actual vehicle behaviour [28,29,31,32].

3.2. Linear vehicle model

The linear vehicle model of the A-double has 5 degrees-of-freedom (DoFs) representing the lateral and yaw motions of the first vehicle unit and the yaw motions of the three towed vehicle units due to the articulation joints. This so-called yaw-plane model is the most common one and has been shown to adequately represent the directional behaviour of vehicles at high speeds (e.g [33–36]). The roll, bounce and pitch dynamics of the vehicle are not included in the formulation. The linear vehicle model is considered to be accurate under the assumption that the steering and articulation angles are small. In addition, the longitudinal velocity of the vehicle is assumed to be constant. The aerodynamic drag, rolling resistance and load transfers are also neglected. Moreover, it is assumed that the vehicle is operating in the tyres' linear region.

A representation of the linear vehicle model is shown in Figure 4, where the axle groups in the semitrailers are lumped together into a single axle in the middle of each axle group. The derivation of the linear model based on Lagrangian formulation is given in Appendix 1. All vehicle parameters are assumed to be known and their values are provided in Appendix 2. The LTI vehicle model is represented with a state-space realisation as

$$\begin{cases} \dot{x}_v(t) = A_v x_v(t) + H_v \delta_{driver}(t) + B_v \delta_{dolly}(t), \\ z(t) = C_v x_v(t) + G_v \delta_{driver}(t) + D_v \delta_{dolly}(t), \\ y(t) = S_v x_v(t) + R_v \delta_{driver}(t), \end{cases} \tag{20}$$

where the state vector $x_v(t) = [\theta_1(t), \theta_2(t), \theta_3(t), v_{y1}(t), \omega_{z1}(t), \dot{\theta}_1(t), \dot{\theta}_2(t), \dot{\theta}_3(t)]^T$ has eight components identified according to the following. $\theta_1(t)$ is the articulation angle between the tractor and the first semitrailer, $\theta_2(t)$ is the articulation angle between the first semitrailer and the dolly; and $\theta_3(t)$ is the articulation angle between the dolly and the last semitrailer. $v_{y1}(t)$ is the lateral velocity of the centre of gravity of the tractor and $\omega_{z1}(t)$ represents the yaw rate of the tractor. The driver input which is identified as the tractor steering angle, $\delta_{driver}(t)$, is viewed in this model as a disturbance input. The control input is indicated by $\delta_{dolly}(t)$, which is the dolly steering angle. In our design exercises, noiseless measurements are considered for simplicity and a single articulation angle is used as the measurement: $y(t) = \theta_2(t)$. The system matrices A_v,H_v, B_v used in the control design are obtained by using a Lagrangian representation (the reader is referred to the Appendix). The matrices C_v, G_v and D_v will be provided in the sequel when the performance evaluation signal is discussed. The matrices S_v and R_v will be defined based on the available measurements. The linear vehicle model has been validated against the nonlinear VTM vehicle model and proved to be sufficiently accurate in predicting the dynamical lateral behaviour [22,37]. It should be remarked that in this work, all parameters and variables of the considered vehicle model for control designs are assumed to be known and measurable or can be estimated. It is possible to design a controller that is robust against the vehicle parameters and variables' variations such as the tyres' cornering stiffness, mass and moments of inertia of the vehicle units and also for varying longitudinal speed (for detailed information refer to the previous works of the authors in [37–39]).

3.2.1. Dolly steering actuator model

The actuator of the dolly steering system is modelled as two parts: a first-order filter with the time constant of τ_a (i.e. $\frac{1}{\tau_a s+1}$) and a transport delay of τ_d (i.e. $e^{-s\tau_\mathrm{d}}$), see also [40]. The transfer function of the time delay is approximated by a first order Padé-approximation (i.e. $e^{-s\tau_d} \approx \frac{1-0.5\tau_\mathrm{d}s}{1+0.5\tau_\mathrm{d}s}$). The dolly steering actuator model is then expressed with a state-space

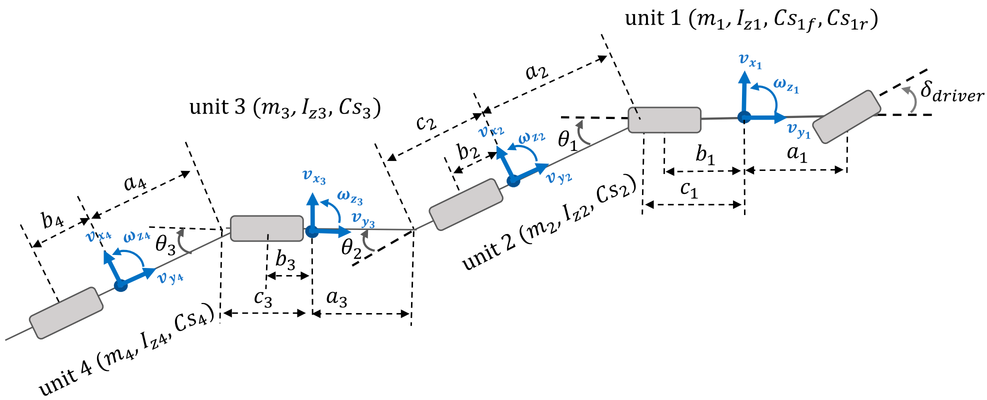

Figure 4. Yaw-plane bicycle model of the A-double.

realisation as

$$
\begin{cases}
\dot{x}_a(t) = \underbrace{\begin{bmatrix} -2/\tau_d & 0 \\ 1/\tau_a & -1/\tau_a \end{bmatrix}}_{A_a} x_a(t) + \underbrace{\begin{bmatrix} 4/\tau_d \\ -1/\tau_a \end{bmatrix}}_{B_a} u(t), \\
\delta_{dolly}(t) = \underbrace{\begin{bmatrix} 0 & 1 \end{bmatrix}}_{C_a} x_a(t) + \underbrace{0}_{D_a} \cdot u(t),
\end{cases}
\tag{21}
$$

where $x_a(t) \in \mathbb{R}^{n_a}$ is the actuator state vector. A new state-space realisation for the full vehicle model is then obtained by appending the steering actuator dynamics to the vehicle model in (20) as follows:

$$
\begin{cases}
\dot{x}_p(t) = \underbrace{\begin{bmatrix} A_v & B_v C_a \\ 0 & A_a \end{bmatrix}}_{A_p} \underbrace{\begin{bmatrix} x_v(t) \\ x_a(t) \end{bmatrix}}_{x_p(t)} + \underbrace{\begin{bmatrix} H_v \\ 0 \end{bmatrix}}_{H_p} \delta_{driver}(t) + \underbrace{\begin{bmatrix} B_v D_a \\ B_a \end{bmatrix}}_{B_p} u(t), \\
z(t) = \underbrace{\begin{bmatrix} C_v & D_v C_a \end{bmatrix}}_{C_p} x_p(t) + \underbrace{G_v}_{G_p} \delta_{driver}(t) + \underbrace{\begin{bmatrix} D_v D_a \end{bmatrix}}_{D_p} u(t), \\
y(t) = \underbrace{\begin{bmatrix} S_v & 0 \end{bmatrix}}_{S_p} x_p(t) + \underbrace{R_v}_{R_p} \delta_{driver}(t),
\end{cases}
\tag{22}
$$

where $x_p(t) \in \mathbb{R}^{n_p}$ with $n_p = n_v + n_a$. In our case study, the actuator parameters are chosen as $\tau_d = 0.1\,s$, and $\tau_a = 0.35\,s$ [40].

3.2.2. Driver model

In order to characterise the typical driver behaviour in single lane change manoeuvres, a simple band-pass model is used to model the frequency content of the driver's steering action. In a single lane change, a human driver is capable of a steering frequency of maximum 3.5 Hz, as stated in [41]. Therefore, the frequency range of 0.05 to 3.5 Hz is chosen for the bandpass filter to represent the driver's steering action in this work. With the Laplace transform of $w(t)$ represented as $\hat{w}(s)$, the tractor steering angle applied by the driver can be expressed in terms of ω_c (center frequency) and ζ (damping ratio) as

$$\hat{\delta}_{driver}(s) = \underbrace{\frac{2\zeta\omega_c s}{s^2 + 2\zeta\omega_c s + \omega_c^2}}_{\mathcal{W}(s)} \hat{w}(s). \tag{23}$$

The centre frequency ω_c is identified as the frequency at which the filter gain is one. A state-space realisation of the bandpass filter can be formed as

$$\begin{cases} \dot{x}_b(t) = \underbrace{\begin{bmatrix} 0 & 1 \\ -\omega_c^2 & -2\zeta\omega_c \end{bmatrix}}_{A_b} x_b(t) + \underbrace{\begin{bmatrix} 0 \\ 2\zeta\omega_c \end{bmatrix}}_{B_b} w(t), \\ \delta_{driver}(t) = \underbrace{\begin{bmatrix} 0 & 1 \end{bmatrix}}_{C_b} x_b(t) + \underbrace{0}_{D_b} \cdot w(t), \end{cases} \tag{24}$$

where $x_b(t) \in \mathbb{R}^{n_b}$ and $w(t)$ are the artificial state vector and disturbance input, respectively. Since a noiseless measurement of $d(t)$ is considered in our design exercises, the model in (24) serves as the input weighting filter introduced in (2) within the problem setting introduced in Section 2. The centre frequency w_c and the bandwidth of the filter can vary depending on the driving style, which can be divided into two categories: typical and aggressive. Hence, if severe avoidance steering inputs happen or an aggressive driver is expected to be modelled, a larger bandwidth should be selected for the filter. In our design exercises for the chosen range of the frequency, a driver model with the parameters $\omega_c = 3.7172\,\text{rad s}^{-1}$ and $\zeta = 1.5945$ are used.

3.3. High-speed lateral performance measures

To evaluate the lateral dynamic performance of the A-double, two different performance measures are used: Rearward Amplification (RA) and High-Speed Transient Off-tracking (HSTO). The RA values can be determined based on frequency- and time-domain approaches recommended by ISO 14791 [42]. The RA based on the time-domain approach is defined as the ratio of the peak value of a desired motion variable (lateral acceleration or yaw rate) of the rearmost unit to that of the lead unit in a specific lane change manoeuvre. This performance measure indicates the combination vehicle's tendency for a rollover or swing out. The HSTO is defined as the maximum lateral path deviation between the front axle of the vehicle and the rearmost axle in the last semitrailer of the combination vehicle. This performance measure is indicating the additional road space required for the last semitrailer during the lane change manoeuvre. It is thus desirable to minimise RA and HSTO to improve the lateral performance of the combination vehicle. Smaller values of RA and HSTO imply better lateral dynamic performance.

3.4. Performance objective in synthesis

The objective of the controller design is to influence the yaw motion of the dolly and the last semitrailer in such a way to improve the lateral dynamic stability of the A-double while preserving stability in transient manoeuvres by employing the active steering of the first axle of the dolly. Therefore, for static output feedback and also joint static output feedback and feed-forward the following performance output syntheses is chosen as

$$z(t) = \begin{bmatrix} \theta_2(t) \\ \theta_3(t) \end{bmatrix} \tag{25}$$

where $\theta_2(t)$ and $\theta_3(t)$ are the second and third articulation angle, respectively. In this fashion, the aim is to suppress undesired oscillations in the second and third articulation angles to suppress unwanted amplified motions in the towed units.

3.5. Synthesis results

In order to illustrate the potential use of the developed synthesis methods, different LTI controller designs are performed; syntheses with SOFB alone and then DFF method combined with SOFB (i.e. SOFB+DFF). The SOFB gain K_{fb} is synthesised by minimising the value of γ under the LMI condition in (9). This is done by performing a line search over ϕ. In the SOFB design, the minimum γ value of 2.04 is obtained around $\phi = 3.80$ with the feedback gain is computed as

$$K_{fb} = -1.5036. \tag{26}$$

In the second step, the DFF matrices (A_f, B_f, C_f, D_f) are computed via single optimizations under LMI conditions. The order l and the pole ψ of the filter are to be chosen by the designer. In this case, the choices $l = 5$ and $\psi = 1$ turned out to be quite convenient values. The transfer function of the synthesised DFF filter is computed as the following:

$$\mathcal{K}_{ff} = \frac{-5.4058(s + 0.1327)(s^2 + 0.5143s + 0.5465)(s^2 + 0.1013s + 2.305)}{(s + 1)^5}, \tag{27}$$

and the associated γ level is 1.87. It is important to note that the γ value is decreased if compared to the one in the SOFB design. This establishes the benefit of using DFF when accurate measurement of the driver steering input is available.

3.6. Simulation results

In this section, the performance of the SOFB and DFF controllers are evaluated in a single lane change (SLC) manoeuvre that is performed by applying a single sine-wave steering as the driver input. In the first step, the yaw rate and lateral acceleration RA values are computed based on time domain simulations performed for a set of different SLC manoeuvres with varying frequency of the driver steering input over a certain range. To have a fair comparison, it is also required to have a peak value of about 1.5 ms^{-2} for the lateral acceleration in the first axle of the tractor and the amplitude of the steering input is adjusted accordingly to provide this level of the lateral acceleration.

The resulting lateral acceleration and yaw rate RA values for the second semitrailer are shown in Figure 5. As can be seen from this figure, adding SOFB controller will suppress the lateral acceleration and yaw rate RA values significantly if compared to the passive case (i.e. no control), and employing DFF controller enhances the performance even more by

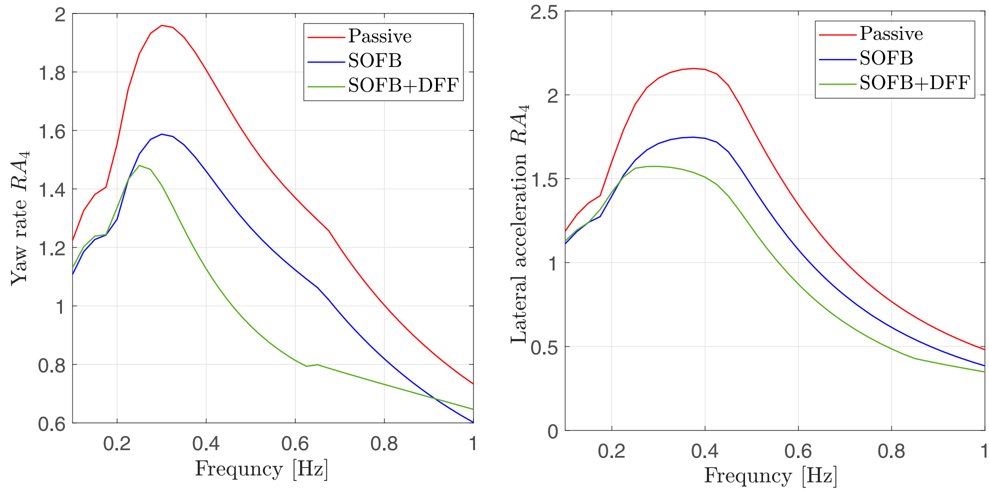

Figure 5. Yaw rate and lateral acceleration RA of the last semitrailer of the VTM vehicle in SLCs ($v_x = 80$ km h^{-1}, peak $|a_{y11}| = 1.5$ ms^{-2}, $\mu = 0.8$).

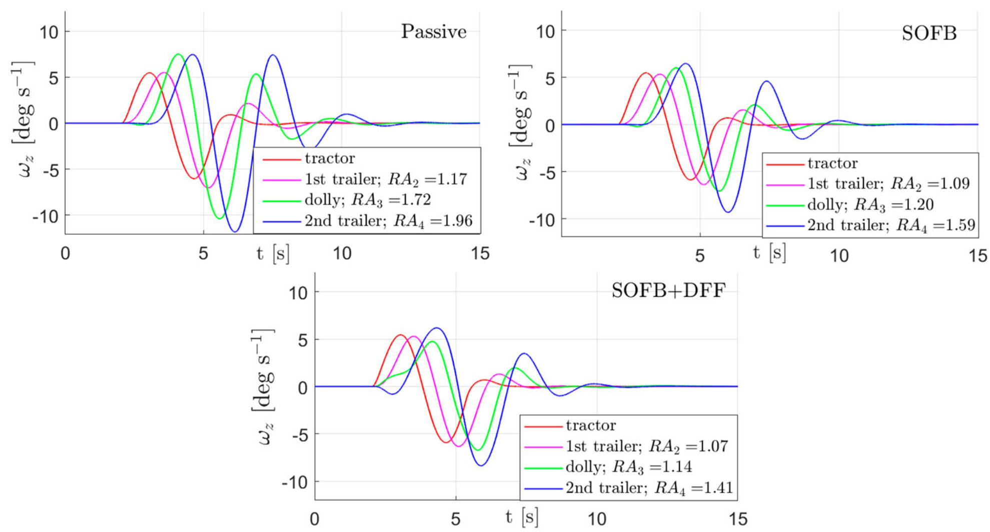

Figure 6. Yaw rates of the units in the VTM vehicle in SLC ($v_x = 80$ km h^{-1}, frequency = 0.3 Hz, peak $|a_{y1}| = 1.5$ ms^{-2}, $\mu = 0.8$).

reducing the RA vales even further for frequencies higher than 0.23 Hz. In the next step, the simulation results are presented for the SLC manoeuvre with the steering frequency of 0.3 Hz for which the yaw rate RA value of the passive vehicle turns out to be the largest in Figure 5.

The yaw rates for the units of the A-double for the passive and active (i.e. controlled) cases are shown in Figure 6. As can be seen, the yaw rate RA of the last semitrailer is 1.96 in the passive A-double. With the application of controllers, the yaw rate RA is decreased to 1.59 and 1.41 for SOFB and SOFB+DFF, respectively. Indeed the yaw rate RA of the last semitrailer is reduced more in the case of SOFB+DFF controller if compared to SOFB

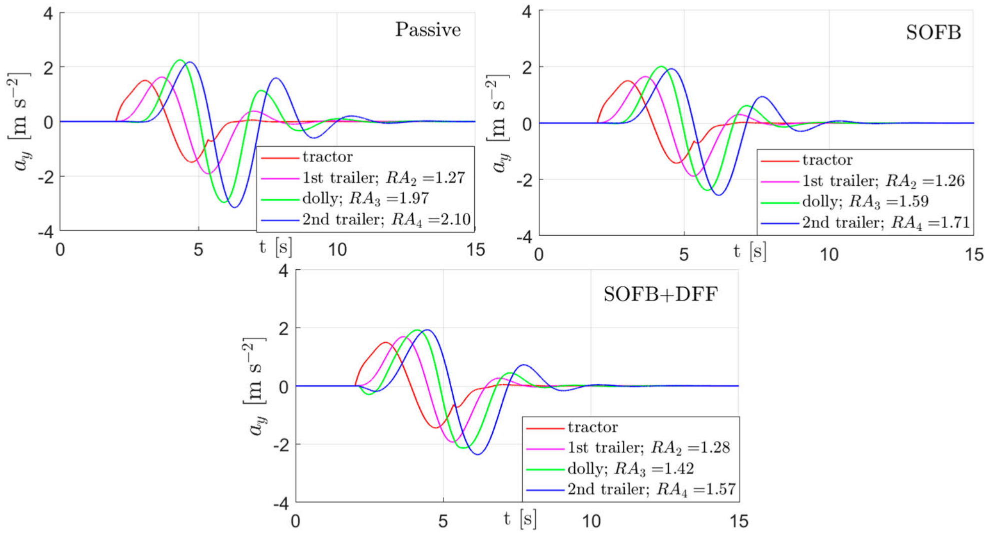

Figure 7. Lateral accelerations of the units in the VTM vehicle in SLC ($v_x = 80$ km h^{-1}, frequency= 0.3 Hz, peak $|a_{y1}| = 1.5$ ms^{-2}, $\mu = 0.8$).

Table 1. Simulation results from SLCs ($v_x = 80$ km h^{-1}, peak $|a_{y1}| = 1.5$ ms^{-2}, frequency $= 0.3$ Hz, $\mu = 0.8$).

	Peak value of yaw rate (deg/s)				Peak value of lateral acceleration (m/s^2)			
Control method	$\|\omega_{z1}\|$	$\|\omega_{z2}\|$	$\|\omega_{z3}\|$	$\|\omega_{z4}\|$	$\|a_{y1}\|$	$\|a_{y2}\|$	$\|a_{y3}\|$	$\|a_{y4}\|$
Passive	6.01	7.01	10.34	11.74	1.50	1.90	2.96	3.15
SOFB	5.86	6.36	6.99	9.28	1.50	1.88	2.39	2.56
SOFB+DFF	5.91	6.31	6.64	8.33	1.50	1.92	2.13	2.35
		Yaw rate RA				Lateral acceleration RA		
Control method		RA_2	RA_3	RA_4		RA_2	RA_3	RA_4
Passive		1.16	1.72	1.95		1.27	1.97	2.10
SOFB		1.09	1.19	1.58		1.26	1.59	1.71
SOFB+DFF		1.07	1.12	1.41		1.28	1.42	1.57

$| * |$: absolute value, ω_{zi}: yaw rate of unit i, a_{yi}: lateral acceleration of unit i

controller as expected. The same reduction pattern is also seen in the case of the lateral acceleration RA as observed in Figure 7. The lateral acceleration RA values of the last semi-trailer in the A-double are 2.10, 1.71 and 1.57 for the passive vehicle, the active vehicle with SOFB controller and the active vehicle with SOFB+DFF controller, respectively. A summary of the simulation results from Figures 6 and 7 is provided in Table 1.

Figure 8 depicts the HSTO values for both passive and active cases. As can be seen from this figure, the HSTO values are decreased from 0.95 m in the passive vehicle to the 0.68 m and 0.62 m in the SOFB and SOFB+DFF controlled cases, respectively. In this performance measure and specific manoeuvre, the SOFB+DFF controller is performing slightly better the SOFB controller.

The steering angle applied by the driver and the dolly steering angle generated by the controllers are shown in Figure 9. As identified from this figure, the reduction in the RA

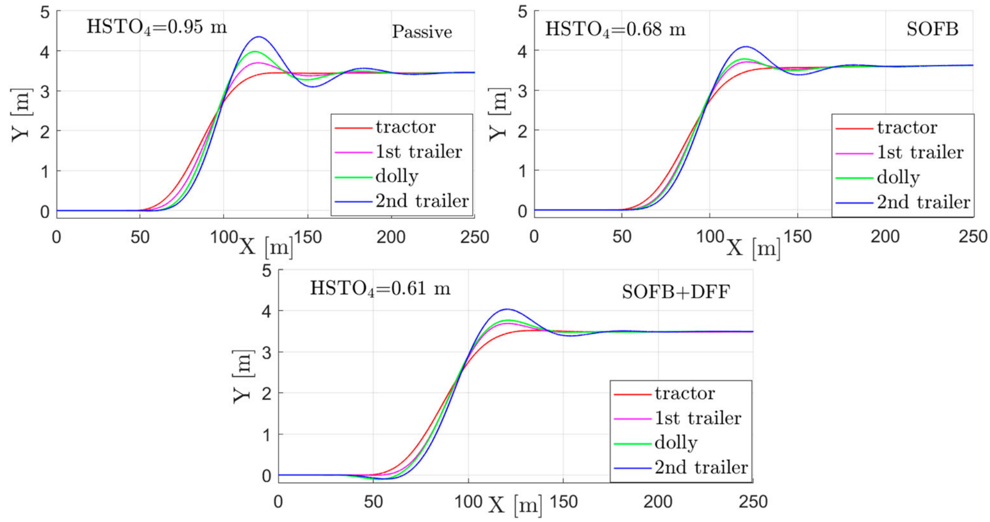

Figure 8. Travelled path of the first axle of the tractor and the centre axle of the units in the VTM vehicle in SLC ($v_x = 80$ km h^{-1}, frequency $= 0.3$ Hz, peak $|a_{y1}| = 1.5$ ms^{-2}, $\mu = 0.8$).

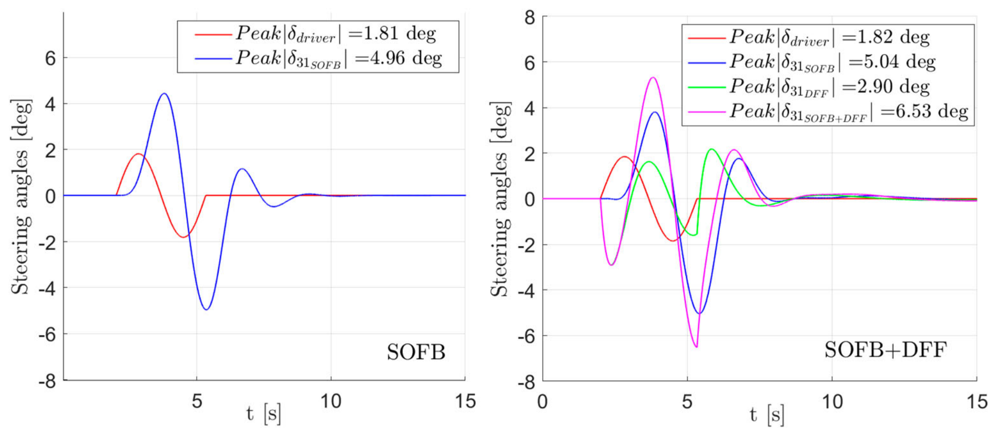

Figure 9. Driver and dolly steering angles of the VTM vehicle in SLC ($v_x = 80$ km h^{-1}, frequency $= 0.3$ Hz, peak $|a_{y1}| = 1.5$ ms^{-2}, $\mu = 0.8$) for the SOFB and SOFB+DFF design cases, δ_{31}: the steering angle of the first axle of the dolly.

values in the controlled cases are achieved by applying dolly steering angles of peak values below 6.6° in the SOFB+DFF controller and below 5.1° in the SOFB controller.

In order to provide a more quantitative evaluation of the performance improvement, Table 2 presents the results obtained for yaw rate RA, as well as lateral acceleration RA and HSTO of the last semitrailer for the vehicle manoeuvring on low-friction and high-friction surfaces. As can be seen from this table, adding DFF to SOFB leads to more attenuation in terms of the yaw rate RA, lateral acceleration RA and HSTO and consequently enhancing the lateral performance further.

It should also be noted, in the case of the passive vehicle manoeuvring on the low-friction surface the lateral acceleration RA indicates an unreasonable value compared to

Table 2. Control methods comparison in SLC ($v_x = 80\,\text{km}\,\text{h}^{-1}$, peak $|a_{y1}| = 1.5\ \text{ms}^{-2}$, frequency = 0.3 Hz) in two different road conditions ($\mu = 0.3, 0.8$).

	RA_4				$HSTO_4$		max $\|\delta_{dolly}\|$	max $\|\delta_{driver}\|$
	ω_z		a_y					
Control method	V* [−]	P+ [%]	V* [−]	P+ [%]	V* [m]	P+ [%]	[deg]	[deg]
Passive, $\mu = 0.8$	1.96	–	2.10	–	0.95	–	0.0	1.81
SOFB, $\mu = 0.8$	1.59	18.88	1.71	18.57	0.68	28.42	4.96	1.81
SOFB+DFF, $\mu = 0.8$	1.41	28.06	1.57	25.24	0.61	35.79	6.53	1.82
Passive, $\mu = 0.3$	2.73	–	1.92	–	1.63	–	0.0	1.91
SOFB, $\mu = 0.3$	1.72	36.76	1.73	10.83	1.08	33.74	6.11	1.90
SOFB+DFF, $\mu = 0.3$	1.58	41.91	1.68	13.40	1.02	37.42	7.72	1.92

∗ :Value, +: Progress

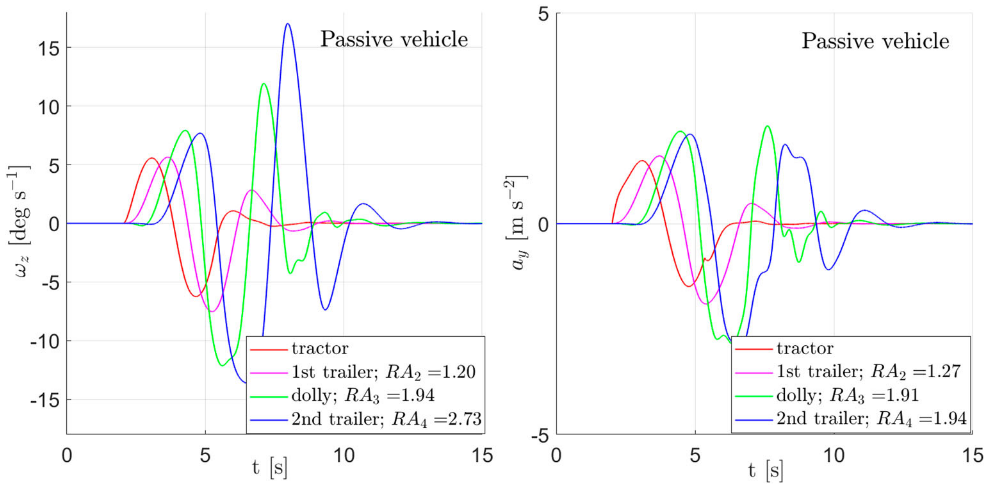

Figure 10. Yaw rate and lateral acceleration of the units of the passive VTM vehicle in SLC ($v_x = 80\,\text{km}\,\text{h}^{-1}$, frequency= 0.3 Hz, peak $|a_{y11}| = 1.5\ \text{ms}^{-2}$, $\mu = 0.3$).

the yaw rate RA. Most often the RA of yaw rate and the RA of lateral acceleration are similar. However, there are some cases in which the use of RA of lateral acceleration as a lateral stability criterion is very misleading. For instance, in a high-speed manoeuvring on a low-friction surface, the RA of yaw rate increases significantly, while the RA of lateral acceleration decreases as observed in our simulations on the low-friction surface as seen in Figure 10. Therefore in such a case, the yaw rate RA is a better performance measure as a lateral stability criterion in high speeds. While in the controlled vehicle as shown in Figure 11, it is observed that by applying the imposed controller, a better agreement can be seen in both the yaw rate and lateral acceleration RA measures if compared to the passive vehicle in a low-friction lane change.

4. Conclusion

In this paper, an LMI-based SOFB synthesis combined with DFF has been developed in order to improve the lateral performance of the A-double vehicle during a high-speed

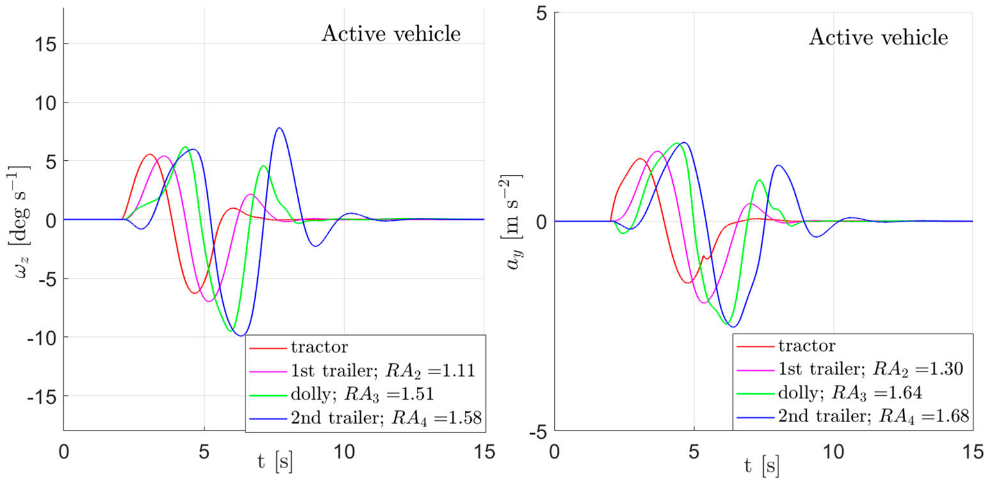

Figure 11. Yaw rate and lateral acceleration of the units of the active VTM vehicle in SLC ($v_x = 80$ km h^{-1}, frequency = 0.3 Hz, peak $|a_{y1}| = 1.5$ ms^{-2}, $\mu = 0.3$).

manoeuvre by only steering the first axle of the dolly. A two-step design methods is proposed in which in the first step an SOFB controller is designed in a way to maintain stability and optimise the performance objective as much as possible. In the second step, a DFF controller is synthesised for the closed-loop system in a way to further optimise the performance objective. The order and the pole(s) of the DFF filter are chosen by the designer beforehand. Both developed synthesis methods (i.e. SOFB and SOFB+DFF) are applied to the control of the A-double to enhance the lateral performance. It is observed that it is possible to reduce the RA and HSTO by SOFB based on the measurements of only the second articulation angle, which from a practical point of view turns out to be the easiest signal to be measured. Even further RA and HSTO reduction are achieved when the DFF from the driver steering angle accompanies the SOFB controller if compared to the case in which DFF is not applied. The driver interaction with the developed controllers is included by considering a simple linear model describing the frequency content of the driver steering in lane change manoeuvres. A more advanced linear driver model could be considered in related future works.

Acknowledgments

The authors would like to thank Hakan Köroğlu for his valuable contribution and support.

Disclosure statement

No potential conflict of interest was reported by the author(s).

Funding

This work was supported by Volvo Group Trucks Technology and Strategic Vehicle Research and Innovation [grantnumber 2017-03036].

ORCID

Maliheh Sadeghi Kati http://orcid.org/0000-0003-3079-4801
Jonas Fredriksson http://orcid.org/0000-0002-9814-6416
Bengt Jacobson http://orcid.org/0000-0002-5798-5651
Leo Laine http://orcid.org/0000-0002-0672-3985

References

[1] Cheng C, Cebon D. Improving roll stability of articulated heavy vehicles using active semi-trailer steering. Vehicle Syst Dyn. 2008;46(sup1):373–388.
[2] Moon KH, Lee SH, Chang S, et al. Method for control of steering angles for articulated vehicles using virtual rigid axles. Int J Automotive Technol. Aug 2009;10:441–449.
[3] Bortoni-Anzures L, Herrera-Ruíz G, Gómez-Meléndez D, et al. Fuzzy controller for automatic steering in heavy vehicle semi-trailers. Ingeniería Investigación y Tecnología; Vol. XIV, 2012. p. 1–9.
[4] Wang Q, He Y. Design validation of active trailer steering systems for improving the low-speed manoeuvrability of multi-trailer articulated heavy vehicles using driver-hardware/software-in-the-loop real-time simulations. Int J Vehicle Performance. 2015;2(1):58–84.
[5] Abroshan M, Taiebat M, Goodarzi A, et al. Automatic steering control in tractor semi-trailer vehicles for low-speed maneuverability enhancement. Proc Institut Mech Eng, Part K: J Multi-body Dyn. 2017;231(1):83–102.
[6] Ding X, He Y, Ren J, et al. A comparative study of control algorithms for active trailer steering systems of articulated heavy vehicles. 2012 American Control Conference (ACC); June 2012. p. 3617–3622.
[7] Rangavajhula K, Tsao H-SJ. Active trailer steering control of an articulated system with a tractor and three full trailers for tractor-track following. Int J Heavy Veh Syst. 2007;14(3):271–293.
[8] Cheng C, Roebuck R, Odhams A, et al. High-speed optimal steering of a tractor-semitrailer. Vehicle Syst Dyn. April 2011;49:561–593.
[9] Kharrazi S. Steering based lateral performance control of long heavy vehicle combinations [PhD thesis]. Gothenburg, Sweden: Chalmers University of Technology; 2012.
[10] Roebuck R, Odhams A, Tagesson K, et al. Implementation of trailer steering control on a multi-unit vehicle at high speeds. ASME. J Dyn Syst, Measurement, and Control. December 2013;136:021016-1–021016-13.
[11] Rangavajhula K, Tsao H-SJ. Command steering of trailers and command-steering-based optimal control of an articulated system for tractor-track following. Proc Institut Mech Eng, Part D: J Automobile Eng. 2008;222(6):935–954.
[12] Odhams AMC, Roebuck RL, Jujnovich BA, et al. Active steering of a tractor-semitrailer. Proc Institut Mech Eng, Part D: J Automobile Eng. 2011;225(7):847–869.
[13] Islam M. Parallel Design Optimization of Multi-Trailer Articulated Heavy Vehicle with Active Safety Systems [Phd thesis]. Oshawa, Ontario, Canada: University of Ontario Institute of Technology; 2013.
[14] Oreh SHT, Kazemi R, Azadi S. Directional control of articulated heavy vehicles. SAE Int J Commercial Vehicles. 2013;6:143–149.
[15] Jujnovich BA, Cebon D. Path-following steering control for articulated vehicles. ASME. J Dyn Syst, Measurement, and Control. 2013;135:031006, 1–031006, 15.
[16] Oreh SHT, Kazemi R, Azadi S. A sliding-mode controller for directional control of articulated heavy vehicles. Proc Instit Mech Eng, Part D: J Automobile Eng. 2014;228(3):245–262.
[17] Milani SA. Modeling, simulation, and active control of tractor-semitrailer combinations [Master thesis]. Mechanical Engineering Department, Middle East Technical University; December 2015.
[18] Kural K, Hatzidimitris P, van de Wouw N, et al. Active trailer steering control for high-capacity vehicle combinations. IEEE Trans Intelligent Vehicles. 2017;2(4):251–265.

[19] Islam MM, Ding X, He Y. A closed-loop dynamic simulation-based design method for articulated heavy vehicles with active trailer steering systems. Vehicle Syst Dyn. 2012;50(5):675–697.
[20] Kural K, Hatzidimitris P, van de Wouw N, et al. Active trailer steering control for high capacity vehicle combinations. IEEE Trans Intelligent Vehicles. 2017;0(99):1–1.
[21] Ding X, Mikaric S, He Y. Design of an active trailer-steering system for multi-trailer articulated heavy vehicles using real-time simulations. Proc Instit Mech Eng, Part D: J Automobile Eng. 2013;227(5):643–655.
[22] Kati MS. On robust steering based lateral control of longer and heavier commercial vehicles [PhD thesis]. Gothenburg, Sweden: Chalmers University of Technology; 2018.
[23] Sadabadi MS, Peaucelle D. From static output feedback to structured robust static output feedback: a survey. Annu Rev Control. 2016;42:11–26.
[24] Köroğlu H, Falcone P. New LMI conditions for static output feedback synthesis with multiple performance objectives. Proc. 53rd IEEE Conference on Decision and Control; Los Angeles, CA: December 15-17 2014. p. 866–871.
[25] Köroğlu H, Falcone P. Joint synthesis of dynamics feed-forward and static state feedback for platoon control. 53rd IEEE Conference on Decision and Control; Los Angeles, California, USA: December 2014.
[26] Kati MS, Köroğlu H, Fredriksson J. Robust lateral control of an A-double combination via $\mathcal{H}_\infty$ and generalized H2 static output feedback. IFAC-PapersOnLine, 8th IFAC Symposium on Advances in Automotive Control AAC, 2016; Vol. 49, No. 11, 2016. p. 305 – 311.
[27] Scherer CW, Gahinet P, Chilali M. Multiobjective output-feedback control via LMI optimisation. Automatic Control, IEEE Trans. 1997;42(7):896–911.
[28] Volvo Group Trcuks Technology. Virtual Truck Model, simulink library develeoped at Volvo Group Trcuks Technology. 2014. Volvo GTT, Department; Tech. rep. (BF72991).
[29] Sundström P, Laine L. Validation of VTM model of tractor 4x2 with semitrailer using winter test results from arjeplog. 2012. p. 2685. Tech. Rep. (2111w11) .
[30] Pacejka H. Tire and vehicle dynamics. Vol. 672, 3rd ed. Butterworth-Heinemann; April 2012.
[31] Kharrazi S, Bruzelius F, Sandberg U. Performance based standards for high capacity transports in Sweden. FIFFI project 2013-03881-Final report VTI rapport 948A, Swedish National Road and Transport Research Institute (VTI), 2017.
[32] Kharrazi S. Performance of high capacity vehicles in winter versus summer. Future pathways: International Symposium on Heavy Vehicle Transport Technology (HVTT14); Rotorua, New Zealand: November 2016.
[33] Pacejka HB. Simplified analysis of steady-state turning behaviour of motor vehicles. part 1. handling diagrams of simple systems. Vehicle Syst Dyn. 1973;2(3):161–172.
[34] Ervin RD, MacAdam CC. The dynamic response of multiply-articulated truck combinations to steering input. West Coast International Meeting and Exposition; SAE International; February 1982.
[35] Fletcher C, Manzie C, Good MC. Trailer Steering : an Australian research perspective and application for by-wire control. 9th International Symposium on Heavy Vehicle Weights and Dimensions; Pennsylvania, USA: International Forum for Road Transport Technology, June 2006.
[36] He Y, Khajepour A, McPhee J, et al. Dynamic modelling and stability analysis of articulated frame steer vehicles. Int J Heavy Veh Syst. 2005;12(1):28–59.
[37] Kati MS, Fredriksson J, Jacobson B, et al. Gain-scheduled $\mathcal{H}_\infty$ controller synthesis for actively steered longer and heavier commercial vehicles. Proc Instit Mech Eng, Part D: J Automobile Eng. 2020;234(7):2045–2065.
[38] Kati MS, Köroğlu H, Fredriksson J. Robust lateral control of heavy combination vehicles under moments of inertia and tire cornering stiffness uncertainties. Vehicle Syst Dyn. 2019;57(12):1847–1873.
[39] Kati MS, Fredriksson J, Jacobson B, et al. Design of a robust load-dependent steering controller for improved high capacity vehicle safety. To appear in 24th IEEE International Conference on Intelligent Transportation-ITSC 2021; Indianapolis, IN, United States: September 2021.

[40] Islam MM, Laine L, Jacobson B. Inverse model control including actuator dynamics for active dolly steering in high capacity transport vehicle. Proc. 2015 IEEE Intelligent Vehicles Symposium (IV); COEX, Seoul, Korea; June 28–July 1 2015. p. 1024–1031.
[41] Powell R. Relationships between lane change performance and open-loop handling metrics. 2009.
[42] Swedish Standards Institute. Road vehicles- Heavy commercial vehicle combinations and articulated buses-Lateral stability test methods. Stockholm, Sweden: 2002. (Svensk Standard SS-ISO 14791 ICS 43.080.01).
[43] Levén M, Sjöblom A, Lidberg M, et al. Derivation of linear single-track truck-dolly-semitrailer model with steerable axles. Department of Applied Mechanics, Chalmers University of Technology; Tech. Rep. September 2011.

Appendices

Appendix 1. Linear model derivation

The linear vehicle model is derived by using Lagrangian equation $\mathcal{M}_q\ddot{q}(t) + \mathcal{C}_q\dot{q}(t) + \mathcal{K}_q q(t) = \mathcal{B}_q\delta_{dolly}(t) + \mathcal{H}_q\delta_{driver}(t)$, where $q^T = [y_1, \varphi_1, \theta_1, \theta_2, \theta_3]$ is the generalised coordinate vector. The system matrices A_q, B_q and H_q are then obtained as follows:

$$\underbrace{\begin{bmatrix}\dot{q}(t)\\ \ddot{q}(t)\end{bmatrix}}_{\dot{x}_q(t)} = \underbrace{\begin{bmatrix}0 & I\\ -\mathcal{M}_q^{-1}\mathcal{K}_q & -\mathcal{M}_q^{-1}\mathcal{C}_q\end{bmatrix}}_{A_q}\underbrace{\begin{bmatrix}q(t)\\ \dot{q}(t)\end{bmatrix}}_{x_q(t)} + \underbrace{\begin{bmatrix}0\\ \mathcal{M}_q^{-1}\mathcal{B}_q\end{bmatrix}}_{B_q}\delta_{dolly}(t) + \underbrace{\begin{bmatrix}0\\ \mathcal{M}_q^{-1}\mathcal{H}_q\end{bmatrix}}_{H_q}\delta_{driver}(t).$$

where the matrices $\mathcal{M}_q$, $\mathcal{C}_q$, $\mathcal{K}_q$, $\mathcal{B}_q$ and $\mathcal{H}_q$ are obtained in terms of the system parameters (see Figure 4). Two states y_1 and φ_1 are removed from x_q to obtain the state-space model to be used in the design. This is possible due to the structure of the matrix $\mathcal{K}_q$. As a result, the state vector is formed as $x_v^T = [\theta_1, \theta_2, \theta_3, v_{y1}, \omega_{z1}, \dot{\theta}_1, \dot{\theta}_2, \dot{\theta}_3]$, where $\omega_{z1} = \dot{\varphi}_1$. By removing the relevant row blocks from all matrices and also the relevant column block from A_q, B_q and H_q, the dynamic of the system is obtained in as $\dot{x}_v = A_v\, x_v + H_v\, \delta_{driver} + B_v\, \delta_{dolly}$. The detailed information about the derivation of the linear vehicle model can be found in [38,43].

The matrices $\mathcal{M}_q, \mathcal{C}_q, \mathcal{K}_q, \mathcal{B}_q$ and $\mathcal{H}_q$ are given in the following. The elements of $\mathcal{M}_q$ (represented as M_{ij}):

$$\begin{aligned}
&M_{11} = m_1 + m_2 + m_3 + m_4,\\
&M_{12} = -m_2(c_1 + a_2) - m_3(c_1 + l_2 + a_3) - m_4(c_1 + l_2 + l_3 + a_4),\\
&M_{13} = -m_2a_2 - m_3(l_2 + a_3) - m_4(l_2 + l_3 + a_4),\\
&M_{14} = -m_3a_3 - m_4(l_3 + a_4), \quad M_{15} = -m_4a_4, \quad M_{21} = M_{12},\\
&M_{22} = J_1 + J_2 + J_3 + J_4 + m_2(c_1 + a_2)^2 + m_3(c_1 + l_2 + a_3)^2 + m_4(c_1 + l_2 + l_3 + a_4)^2,\\
&M_{23} = J_2 + J_3 + J_4 + m_2a_2(c_1 + a_2) + m_3(l_2 + a_3)(c_1 + l_2 + a_3),\\
&\qquad\quad + m_3(l_2 + a_3)(c_1 + l_2 + a_3) + m_4(l_2 + l_3 + a_4)(c_1 + l_2 + l_3 + a_4),\\
&M_{24} = J_3 + J_4 + m_3a_3(c_1 + l_2 + a_3) + m_4(l_3 + a_4)(c_1 + l_2 + l_3 + a_4),\\
&M_{25} = J_4 + m_4a_4(c_1 + l_2 + l_3 + a_4), \quad M_{31} = M_{13}, \quad M_{32} = M_{23},\\
&M_{33} = J_2 + J_3 + J_4 + m_2a_2^2 + m_3(l_2 + a_3)^2 + m_4(l_2 + l_3 + a_4)^2,\\
&M_{34} = J_3 + J_4 + m_3a_3(l_2 + a_3) + m_4(l_3 + a_4)(l_2 + l_3 + a_4),\\
&M_{35} = J_4 + m_4a_4(l_2 + l_3 + a_4), \quad M_{41} = M_{14}, \quad M_{42} = M_{24}, \quad M_{43} = M_{34},\\
&M_{44} = J_3 + J_4 + m_3a_3^2 + m_4(l_3 + a_4)^2, \quad M_{45} = J_4 + m_4a_4(l_3 + a_4),\\
&M_{51} = M_{15}, \quad M_{52} = M_{25}, \quad M_{53} = M_{35}, \quad M_{54} = M_{45}, \quad M_{55} = I_{z4} + m_4a_4^2,
\end{aligned}$$

where $l_2 = a_2 + c_2$ and $l_3 = a_3 + c_3$. The elements of $\mathcal{K}_q$ (represented as K_{ij}):

$$K_{11} = K_{12} = K_{21} = K_{22} = K_{31} = K_{32} = K_{41} = K_{42} = K_{51} = K_{52} = 0,$$
$$K_{13} = -(Cs_2 + Cs_{31} + Cs_{32} + Cs_4), \quad K_{14} = -(Cs_{31} + Cs_{32} + Cs_4), \quad K_{15} = -Cs_4,$$
$$K_{23} = Cs_2(c_1 + a_2 + b_2) + Cs_{31}(c_1 + l_2 + a_3 + b_{31}) + Cs_{32}(c_1 + l_2 + a_3 + b_{32}),$$
$$+ Cs_4(c_1 + l_2 + l_3 + a_4 + b_4),$$
$$K_{24} = Cs_{31}(c_1 + l_2 + a_3 + b_{31}) + Cs_{32}(c_1 + l_2 + a_3 + b_{32}) + Cs_4(c_1 + l_2 + l_3 + a_4 + b_4),$$
$$K_{25} = Cs_4(c_1 + l_2 + l_3 + a_4 + b_4),$$
$$K_{33} = Cs_2(a_2 + b_2) + Cs_{31}(l_2 + a_3 + b_{31}) + Cs_{32}(l_2 + a_3 + b_{32}) + Cs_4(l_2 + l_3 + a_4 + b_4),$$
$$K_{34} = Cs_{31}(l_2 + a_3 + b_{31}) + Cs_{32}(l_2 + a_3 + b_{32}) + Cs_4(l_2 + l_3 + a_4 + b_4),$$
$$K_{35} = Cs_4(l_2 + l_3 + a_4 + b_4), \quad K_{53} = K_{54} = K_{55} = Cs_4(a_4 + b_4).$$

The elements of $\mathcal{C}_q$ (represented as C_{ij}):

$$C_{11} = (Cs_{11} + Cs_{12} + Cs_2 + Cs_{31} + Cs_{32} + Cs_4)/v_x,$$
$$C_{12} = (m_1 + m_2 + m_3 + m_4)v_x - (-Cs_{11}a_1 + Cs_{12}b_1 + Cs_2(c_1 + a_2 + b_2),$$
$$+ C_{31}(c_1 + l_2 + a_3 + b_{31}) + C_{32}(c_1 + l_2 + a_3 + b_{32}) + Cs_4(c_1 + l_2 + l_3 + a_4 + b_4))/v_x,$$
$$C_{13} = -(Cs_2(a_2 + b_2) + Cs_{31}(l_2 + a_3 + b_{31}) + Cs_{32}(l_2 + a_3 + b_{32}) + Cs_4(l_2 + l_3 + a_4 + b_4))/v_x,$$
$$C_{14} = -(Cs_{31}(a_3 + b_{31}) + Cs_{32}(a_3 + b_{32}) + Cs_4(l_3 + a_4 + b_4))/v_x, \; C_{15} = -Cs_4(a_4 + b_4)/v_x,$$
$$C_{21} = -(-Cs_{11}a_1 + Cs_{12}b_1 + Cs_2(c_1 + a_2 + b_2) + Cs_{31}(c_1 + l_2 + a_3 + b_{31}),$$
$$+ Cs_{32}(c_1 + l_2 + a_3 + b_{32}) + Cs_4(c_1 + l_2 + l_3 + a_4 + b_4))/v_x,$$
$$C_{22} = -(m_2(c_1 + a_2) + m_3(c_1 + l_2 + a_3) + m_4(c_1 + l_2 + l_3 + a_4))v_x,$$
$$+ (Cs_{11}a_1^2 + Cs_{21}b_2^2 + Cs_2(c_1 + a_2 + b_2)^2 + Cs_{31}(c_1 + l_2 + a_3 + b_{31})^2,$$
$$+ Cs_{32}(c_1 + l_2 + a_3 + b_{32})^2 + Cs_4(c_1 + l_2 + l_3 + a_4 + b_4)^2)/v_x,$$
$$C_{23} = (Cs_2(a_2 + b_2)(a_1 + a_2 + b_2) + Cs_{31}(l_2 + a_3 + b_{31})(a_1 + l_2 + a_3 + b_{31}),$$
$$+ Cs_{32}(l_2 + a_3 + b_{31})(a_1 + l_2 + a_3 + b_{32})$$
$$+ Cs_4(l_2 + l_3 + a_4 + b_4)(a_1 + l_2 + l_3 + a_4 + b_4))/v_x,$$
$$C_{24} = (Cs_{31}(a_3 + b_{31})(a_1 + l_2 + a_3 + b_{31}) + Cs_{32}(a_3 + b_{32})(a_1 + l_2 + a_3 + b_{32}),$$
$$+ Cs_4(l_3 + a_4 + b_4)(a_1 + l_2 + l_3 + a_4 + b_4))/v_x,$$
$$C_{25} = Cs_4(a_4 + b_4)(a_1 + l_2 + l_3 + a_4 + b_4)/v_x, \quad C_{31} = C_{13}, \quad C_{32} = C_{23},$$
$$C_{33} = (Cs_2(a_2 + b_2)^2 + Cs_{31}(l_2 + a_3 + b_{31})^2 + Cs_{32}(l_2 + a_3 + b_{32})^2$$
$$+ Cs_4(l_2 + l_3 + a_4 + b_4)^2)/v_x,$$
$$C_{34} = (Cs_{31}(a_3 + b_{31})(l_2 + a_3 + b_{31}) + Cs_{32}(a_3 + b_{32})(l_2 + a_3 + b_{32})$$
$$+ Cs_4(l_3 + a_4 + b_4)(l_2 + l_3 + a_4 + b_4))/v_x,$$
$$C_{35} = Cs_4(a_4 + b_4)(l_2 + l_3 + a_4 + b_4)/v_x,$$
$$C_{41} = (Cs_{31}(a_3 + b_{31}) + Cs_{32}(a_3 + b_{32}) + Cs_4(l_3 + a_4 + b_4))/v_x,$$
$$C_{42} = C_{24} - (m_3a_3 + m_4(l_3 + a_4))v_x, C_{43} = C_{34}, \quad C_{51} = C_{15},$$
$$C_{44} = (Cs_3(a_3 + b_3)^2 + Cs_4(l_3 + a_4 + b_4)^2)/v_x, C_{45} = C_4l_4(l_3 + a_4 + b_4))/v_x,$$
$$C_{52} = C_{25} - m_4a_4v_x, \quad C_{53} = C_{35}, \quad C_{54} = C_{45}, \quad C_{55} = Cs_4(a_4 + b_4)^2/v_x.$$

Table A1. Vehicle model parameters.

Parameter	Value	Unit
m_1, m_2, m_3, m_4	9309, 31023, 4300, 31023	kg
J_1, J_2, J_3, J_4	43257, 462660, 7431, 462660	kg m^2
$Cs_{11}, Cs_{12}, Cs_2, Cs_{31}, Cs_{32}, Cs_4$	375120, 476020, 1517800, 524370, 524370, 1465000	N rad^{-1}
a_1, a_2, a_3, a_4	1.5963, 5.2515, 4.3814, 5.2515	m
$b_1, b_2, b_{31}, b_{32}, b_4$	2.4887, 2.8585, 0.3314, 0.9886, 2.855	m
c_1, c_2, c_3	2.1037, 5.2685, 0.1736	m

The matrices $\mathcal{B}_q$ and $\mathcal{H}_q$ are calculated as follows:

$$\mathcal{B}_q^T = \begin{bmatrix} Cs_{31} & -Cs_{31}(c_1 + l_2 + a_3 + b_{31}) & -Cs_{31}(l_2 + a_3 + b_{31}) & -Cs_{31}(a_3 + b_{31}) & 0 \end{bmatrix},$$
$$\mathcal{H}_q^T = \begin{bmatrix} Cs_{11} & Cs_{11}a_1 & 0 & 0 & 0 \end{bmatrix}.$$

Appendix 2. Vehicle Parameters

The vehicle parameters used in the linear vehicle model are listed in Table A1.

In this table, m_i and J_i are the mass and the yaw moment of inertia of the unit i, respectively. Cs_{11} and Cs_{11} are the tire cornering stiffness of the front and rear axles of the tractor, respectively. Cs_2 and Cs_4 are the total tire cornering stiffness for the first and second semitrailer, respectively. Cs_{31} and Cs_{32} are the cornering stiffness of the tyres on the first and second axles of the dolly, respectively. a_i indicates the distance between the centre of gravity (CoG) and the first axle of the unit i, b_i is the distance between CoG and centre of rear axles group of the unit i, c_i is the distance between CoG and the rear coupling point of the unit i.